Elliptic Flow in Au + Au Collisions at $\sqrt{s_{NN}} = 130$ GeV

K. H. Ackermann,[19] N. Adams,[28] C. Adler,[12] Z. Ahammed,[27] S. Ahmad,[28] C. Allgower,[13] J. Amsbaugh,[34]
M. Anderson,[6] E. Anderssen,[17] H. Arnesen,[3] L. Arnold,[14] G. S. Averichev,[10] A. Baldwin,[16] J. Balewski,[13]
O. Barannikova,[10,27] L. S. Barnby,[16] J. Baudot,[14] M. Beddo,[1] S. Bekele,[24] V. V. Belaga,[10] R. Bellwied,[35] S. Bennett,[35]
J. Bercovitz,[17] J. Berger,[12] W. Betts,[24] H. Bichsel,[34] F. Bieser,[17] L. C. Bland,[13] M. Bloomer,[17] C. O. Blyth,[4] J. Boehm,[17]
B. E. Bonner,[28] D. Bonnet,[14] R. Bossingham,[17] M. Botlo,[3] A. Boucham,[30] N. Bouillo,[30] S. Bouvier,[30] K. Bradley,[17]
F. P. Brady,[6] E. S. Braithwaite,[2] W. Braithwaite,[2] A. Brandin,[21] R. L. Brown,[3] G. Brugalette,[34] C. Byrd,[2] H. Caines,[24]
M. Calderón de la Barca Sánchez,[36] A. Cardenas,[27] L. Carr,[34] J. Carroll,[17] J. Castillo,[30] B. Caylor,[17] D. Cebra,[6]
S. Chatopadhyay,[35] M. L. Chen,[3] W. Chen,[3] Y. Chen,[7] S. P. Chernenko,[10] M. Cherney,[9] A. Chikanian,[36] B. Choi,[31]
J. Chrin,[9] W. Christie,[3] J. P. Coffin,[14] L. Conin,[30] C. Consiglio,[3] T. M. Cormier,[35] J. G. Cramer,[34] H. J. Crawford,[5]
V. I. Danilov,[10] D. Dayton,[3] M. DeMello,[28] W. S. Deng,[16] A. A. Derevschikov,[26] M. Dialinas,[30] H. Diaz,[3]
P. A. DeYoung,[8] L. Didenko,[3] D. Dimassimo,[3] J. Dioguardi,[3] W. Dominik,[32] C. Drancourt,[30] J. E. Draper,[6]
V. B. Dunin,[10] J. C. Dunlop,[36] V. Eckardt,[19] W. R. Edwards,[17] L. G. Efimov,[10] T. Eggert,[19] V. Emelianov,[21]
J. Engelage,[5] G. Eppley,[28] B. Erazmus,[30] A. Etkin,[3] P. Fachini,[29] C. Feliciano,[3] D. Ferenc,[6] M. I. Ferguson,[7]
H. Fessler,[19] E. Finch,[36] V. Fine,[3] Y. Fisyak,[3] D. Flierl,[12] I. Flores,[5] K. J. Foley,[3] D. Fritz,[17] N. Gagunashvili,[10]
J. Gans,[36] M. Gazdzicki,[12] M. Germain,[14] F. Geurts,[28] V. Ghazikhanian,[7] C. Gojak,[14] J. Grabski,[33] O. Grachov,[35]
M. Grau,[3] D. Greiner,[17] L. Greiner,[5] V. Grigoriev,[21] D. Grosnick,[1] J. Gross,[9] G. Guilloux,[30] E. Gushin,[21] J. Hall,[35]
T. J. Hallman,[3] D. Hardtke,[17] G. Harper,[34] J. W. Harris,[36] P. He,[5] M. Heffner,[6] S. Heppelmann,[25] T. Herston,[27] D. Hill,[1]
B. Hippolyte,[14] A. Hirsch,[27] E. Hjort,[27] G. W. Hoffmann,[31] M. Horsley,[36] M. Howe,[34] H. Z. Huang,[7] T. J. Humanic,[24]
H. Hümmler,[19] W. Hunt,[13] J. Hunter,[17] G. J. Igo,[7] A. Ishihara,[31] Yu. I. Ivanshin,[11] P. Jacobs,[17] W. W. Jacobs,[13]
S. Jacobson,[17] R. Jared,[17] P. Jensen,[31] I. Johnson,[17] P. G. Jones,[4] E. Judd,[5] M. Kaneta,[17] M. Kaplan,[8] D. Keane,[16]
V. P. Kenney,[23,*] A. Khodinov,[21] J. Klay,[6] S. R. Klein,[17] A. Klyachko,[13] G. Koehler,[17] A. S. Konstantinov,[26]
V. Kormilitsyne,[7,26] L. Kotchenda,[21] I. Kotov,[24] A. D. Kovalenko,[10] M. Kramer,[22] P. Kravtsov,[21] K. Krueger,[1]
T. Krupien,[3] P. Kuczewski,[3] C. Kuhn,[14] G. J. Kunde,[36] C. L. Kunz,[8] R. Kh. Kutuev,[11] A. A. Kuznetsov,[10]
L. Lakehal-Ayat,[30] J. Lamas-Valverde,[28] M. A. C. Lamont,[4] J. M. Landgraf,[3] S. Lange,[12] C. P. Lansdell,[31] B. Lasiuk,[36]
F. Laue,[24] A. Lebedev,[3] T. LeCompte,[1] W. J. Leonhardt,[3] V. M. Leontiev,[26] P. Leszczynski,[33] M. J. LeVine,[3] Q. Li,[35]
Q. Li,[17] Z. Li,[3] C.-J. Liaw,[3] J. Lin,[9] S. J. Lindenbaum,[22] V. Lindenstruth,[5] P. J. Lindstrom,[5] M. A. Lisa,[24] H. Liu,[16]
T. Ljubicic,[3] W. J. Llope,[28] G. LoCurto,[19] H. Long,[7] R. S. Longacre,[3] M. Lopez-Noriega,[24] D. Lopiano,[1] W. A. Love,[3]
J. R. Lutz,[14] D. Lynn,[3] L. Madansky,[15,*] R. Maier,[19] R. Majka,[36] A. Maliszewski,[33] S. Margetis,[16] K. Marks,[17]
R. Marstaller,[19] L. Martin,[30] J. Marx,[17] H. S. Matis,[17] Yu. A. Matulenko,[26] E. A. Matyushevski,[10] C. McParland,[17]
T. S. McShane,[9] J. Meier,[9] Yu. Melnick,[26] A. Meschanin,[26] P. Middlekamp,[3] N. Mikhalin,[7,26] B. Miller,[3]
Z. Milosevich,[8] N. G. Minaev,[26] B. Minor,[17] J. Mitchell,[15] E. Mogavero,[3] V. A. Moiseenko,[11] D. Moltz,[17] C. F. Moore,[31]
V. Morozov,[17] R. Morse,[17] M. M. de Moura,[29] M. G. Munhoz,[29] G. S. Mutchler,[28] J. M. Nelson,[4] P. Nevski,[3]
T. Ngo,[7] M. Nguyen,[3] T. Nguyen,[3] V. A. Nikitin,[11] L. V. Nogach,[26] T. Noggle,[17] B. Norman,[16] S. B. Nurushev,[26]
T. Nussbaum,[28] J. Nystrand,[17] G. Odyniec,[17] A. Ogawa,[25] C. A. Ogilvie,[18] K. Olchanski,[3] M. Oldenburg,[19]
D. Olson,[17] G. A. Ososkov,[10] G. Ott,[31] D. Padrazo,[3] G. Paic,[24] S. U. Pandey,[35] Y. Panebratsev,[10] S. Y. Panitkin,[16]
A. I. Pavlinov,[26] T. Pawlak,[33] M. Pentia,[10] V. Perevotchikov,[3] W. Peryt,[33] V. A Petrov,[11] W. Pinganaud,[30] S. Pirogov,[7]
E. Platner,[28] J. Pluta,[33] I. Polk,[3] N. Porile,[27] J. Porter,[3] A. M. Poskanzer,[17] E. Potrebenikova,[10] D. Prindle,[34]
C. Pruneau,[35] J. Puskar-Pasewicz,[13] G. Rai,[17] J. Rasson,[17] O. Ravel,[30] R. L. Ray,[31] S. V. Razin,[10,13] D. Reichhold,[9]
J. Reid,[34] R. E. Renfordt,[12] F. Retiere,[30] A. Ridiger,[21] J. Riso,[35] H. G. Ritter,[17] J. B. Roberts,[28] D. Roehrich,[12]
O. V. Rogachevski,[10] J. L. Romero,[6] C. Roy,[30] D. Russ,[8] V. Rykov,[35] I. Sakrejda,[17] R. Sanchez,[7] Z. Sandler,[7]
J. Sandweiss,[36] P. Sappenfield,[28] A. C. Saulys,[3] I. Savin,[11] J. Schambach,[31] R. P. Scharenberg,[27] J. Scheblien,[3]
R. Scheetz,[3] R. Schlueter,[17] N. Schmitz,[19] L. S. Schroeder,[17] M. Schulz,[3,19] A. Schüttauf,[19] J. Sedlmeir,[3] J. Seger,[9]
D. Seliverstov,[21] J. Seyboth,[19] P. Seyboth,[19] R. Seymour,[34] E. I. Shakaliev,[10] K. E. Shestermanov,[26] Y. Shi,[7]
S. S. Shimanskii,[10] D. Shuman,[17] V. S. Shvetcov,[11] G. Skoro,[10] N. Smirnov,[36] L. P. Smykov,[10] R. Snellings,[17]
K. Solberg,[13] J. Sowinski,[13] H. M. Spinka,[1] B. Srivastava,[27] E. J. Stephenson,[13] R. Stock,[12] A. Stolpovsky,[35] N. Stone,[3]
R. Stone,[17] M. Strikhanov,[21] B. Stringfellow,[27] H. Stroebele,[12] C. Struck,[12] A. A. P. Suaide,[29] E. Sugarbaker,[24]
C. Suire,[14] T. J. M. Symons,[17] J. Takahashi,[29] A. H. Tang,[16] A. Tarchini,[14] J. Tarzian,[17] J. H. Thomas,[17] V. Tikhomirov,[21]
A. Szanto de Toledo,[29] S. Tonse,[17] T. Trainor,[34] S. Trentalange,[7] M. Tokarev,[10] M. B. Tonjes,[20] V. Trofimov,[21]

O. Tsai,[7] K. Turner,[3] T. Ullrich,[36] D. G. Underwood,[1] I. Vakula,[7] G. Van Buren,[3] A. M. VanderMolen,[20]
A. Vanyashin,[17] I. M. Vasilevski,[11] A. N. Vasiliev,[26] S. E. Vigdor,[13] G. Visser,[5] S. A. Voloshin,[35] C. Vu,[17] F. Wang,[27]
H. Ward,[31] D. Weerasundara,[34] R. Weidenbach,[17] R. Wells,[17] R. Wells,[24] T. Wenaus,[3] G. D. Westfall,[20] J. P. Whitfield,[8]
C. Whitten, Jr.,[7] H. Wieman,[17] R. Willson,[24] K. Wilson,[35] J. Wirth,[17] J. Wisdom,[7] S. W. Wissink,[13] R. Witt,[16] J. Wolf,[17]
L. Wood,[6] N. Xu,[17] Z. Xu,[36] A. E. Yakutin,[26] E. Yamamoto,[7] J. Yang,[7] P. Yepes,[28] A. Yokosawa,[1] V. I. Yurevich,[10]
Y. V. Zanevski,[10] J. Zhang,[17] W. M. Zhang,[16] J. Zhu,[34] D. Zimmerman,[17] R. Zoulkarneev,[11] and A. N. Zubarev[10]

(STAR Collaboration)

[1]*Argonne National Laboratory, Argonne, Illinois 60439*
[2]*University of Arkansas, Little Rock, Arkansas 72204*
[3]*Brookhaven National Laboratory, Upton, New York 11973*
[4]*University of Birmingham, Birmingham, United Kingdom*
[5]*University of California, Berkeley, California 94720*
[6]*University of California, Davis, California 95616*
[7]*University of California, Los Angeles, California 90095*
[8]*Carnegie Mellon University, Pittsburgh, Pennsylvania 15213*
[9]*Creighton University, Omaha, Nebraska 68178*
[10]*Laboratory for High Energy (JINR), Dubna, Russia*
[11]*Particle Physics Laboratory (JINR), Dubna, Russia*
[12]*University of Frankfurt, Frankfurt, Germany*
[13]*Indiana University, Bloomington, Indiana 47408*
[14]*Institut de Recherches Subatomiques, Strasbourg, France*
[15]*The Johns Hopkins University, Baltimore, Maryland 21218*
[16]*Kent State University, Kent, Ohio 44242*
[17]*Lawrence Berkeley National Laboratory, Berkeley, California 94720*
[18]*Massachusetts Institute of Technology, Cambridge, Massachusetts 02139*
[19]*Max-Planck-Institut fuer Physik, Munich, Germany*
[20]*Michigan State University, East Lansing, Michigan 48824*
[21]*Moscow Engineering Physics Institute, Moscow, Russia*
[22]*City College of New York, New York City, New York 10031*
[23]*University of Notre Dame, Notre Dame, Indiana 46556*
[24]*The Ohio State University, Columbus, Ohio 43210*
[25]*Pennsylvania State University, University Park, Pennsylvania 16802*
[26]*Institute of High Energy Physics, Protvino, Russia*
[27]*Purdue University, West Lafayette, Indiana 47907*
[28]*Rice University, Houston, Texas 77251*
[29]*Universidade de Sao Paulo, Sao Paulo, Brazil*
[30]*SUBATECH, Nantes, Nantes, France*
[31]*University of Texas, Austin, Texas 78712*
[32]*Warsaw University, Warsaw, Poland*
[33]*Warsaw University of Technology, Warsaw, Poland*
[34]*University of Washington, Seattle, Washington 98185*
[35]*Wayne State University, Detroit, Michigan 48201*
[36]*Yale University, New Haven, Connecticut 06520*
(Received 13 September 2000)

Elliptic flow from nuclear collisions is a hadronic observable sensitive to the early stages of system evolution. We report first results on elliptic flow of charged particles at midrapidity in Au + Au collisions at $\sqrt{s_{NN}} = 130$ GeV using the STAR Time Projection Chamber at the Relativistic Heavy Ion Collider. The elliptic flow signal, v_2, averaged over transverse momentum, reaches values of about 6% for relatively peripheral collisions and decreases for the more central collisions. This can be interpreted as the observation of a higher degree of thermalization than at lower collision energies. Pseudorapidity and transverse momentum dependence of elliptic flow are also presented.

The goal of the ultrarelativistic nuclear collision program is the creation of a system of deconfined quarks and gluons [1]. If this system is created, its evolution should be governed by the physics of deconfined matter. Elliptic flow, which is sensitive to the early evolution of the system, is the anisotropic emission of particles "in" or "out" of

the reaction plane defined for noncentral collisions by the beam direction (z axis) and the impact parameter direction (x axis). The word flow is used to describe collective behavior but does not necessarily imply a hydrodynamic interpretation. Elliptic flow is usually characterized in terms of particle momenta by $v_2 = \langle (p_x^2 - p_y^2)/(p_x^2 + p_y^2) \rangle$,

the second harmonic Fourier coefficient in the azimuthal distribution of particles with respect to the reaction plane [2,3]. Elliptic flow has its origin in the spatial anisotropy of the system when it is created in a noncentral collision, and in particle rescatterings in the evolving system which convert the spatial anisotropy to momentum anisotropy. The spatial anisotropy in general decreases with system expansion, thus quenching this effect and making elliptic flow particularly sensitive to the early stages of the system evolution [4]. Being dependent on rescattering, elliptic flow is sensitive to the degree of thermalization of the system [5,6] at this early time. Hydrodynamic models, which are based on the assumption of complete local thermalization, predict the strongest signals [6–9].

Elliptic flow in ultrarelativistic nuclear collisions was first discussed in Ref. [7] and has been studied intensively in recent years at the Alternating Gradient Synchrotron (AGS) [10,11] and the CERN Super Proton Synchrotron (SPS) [12–14] energies. These studies have found that elliptic flow at high energies is "in plane," $v_2 > 0$, as expected from most models, and the pion elliptic flow for relatively peripheral collisions increases with beam energy [15] from about 2% at the top AGS energy [10] to about 3.5% at the SPS [13]. From transport cascade models for the full Relativistic Heavy Ion Collider (RHIC) energy, a peak elliptic flow value of 1.5% is predicted by ultra-relativistic quantum molecular dynamics [16] calculations and 2.5% by relativistic quantum molecular dynamics v2.4 [17] calculations [18]. Hydrodynamic models predict v_2 as high as 10% [6,8]. Details of the v_2 dependence on beam energy and centrality are thought to be sensitive to the phase transition between confined and deconfined matter [5,6,8,9,19] (see also [15], and references therein).

We report here the first results on elliptic flow in Au + Au collisions at RHIC at $\sqrt{s_{NN}} = 130$ GeV. The Solenoidal Tracker at RHIC (STAR) [20] consists of several detector subsystems in a large solenoidal magnet. For first year data taking, the setup consists of the Time Projection Chamber (TPC) which covers the pseudorapidity range $|\eta| < 1.8$ for collisions in the center of the TPC, and has complete azimuthal coverage, which is desirable for the study of azimuthal correlations. In the first year, the TPC is operated with a 0.25 T field, allowing tracking of particles with $p_t > 75$ MeV/c. Two zero degree calorimeters [21] which measure fragmentation neutrons are used in coincidence for the trigger. The TPC is surrounded by a scintillator barrel which measures the charged particle multiplicity, and is used in studies of the trigger performance and vertex reconstruction efficiency.

The relative multiplicity distribution for events with a reconstructed primary vertex is shown in Fig. 1. An analysis of the trigger performance and vertex reconstruction efficiency, together with comparisons with Hijing [22], shows that the events in Fig. 1 are hadronic Au + Au interactions corresponding to about 80% to 90% of the geometric cross section, the losses being due to vertex reconstruction inefficiency for low multiplicity events. This inefficiency
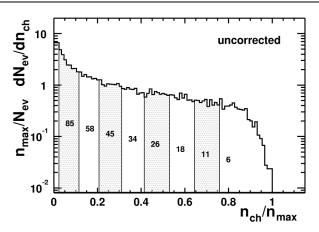

FIG. 1. The primary track multiplicity distribution as a function of the number of tracks normalized by the maximum observed number of tracks. The eight centrality regions used in this analysis are shown. The integral under the curve is 1.0 and the cumulative fraction corresponding to the lower edge of each centrality bin is also indicated in percent.

is not included in the normalization of Fig. 1. The multiplicity is the number of primary tracks which pass within 3 cm of the vertex and have $|\eta| < 0.75$. The distribution shown is not corrected for tracking efficiency; it is used in this analysis only to estimate centralities.

For this analysis, 22 k events were selected with a primary vertex position within 75 cm longitudinally of the TPC center and within 1 cm radially of the beam line. Tracks were selected with $0.1 < p_t \leq 2.0$ GeV/c in order to have a tracking efficiency constant to within $\pm 10\%$. They also passed within 1 cm of the primary vertex, had at least 15 space points, and $|\eta| < 1.3$. For the determination of the event plane we required $|\eta| < 1.0$. Also, the ratio of the number of space points to the expected maximum number of space points for that particular track was required to be greater than 0.52, largely suppressing split tracks from being counted twice. However, the analysis results are not sensitive to these cuts.

The analysis method [2,3] involves the calculation of the event plane angle, which is an experimental estimator of the real reaction plane angle. The second harmonic event plane angles, Ψ_2, are calculated for two subevents, which are groups of independent particles from the same event. In order to see whether these planes are correlated, the mean cosine of the difference in their event plane angles is calculated. Although the STAR detector has good azimuthal symmetry, small acceptance effects in the calculation of the event plane angle were removed by the methods of shifting or weighting [3]. This correction, by either method, is negligible for the second harmonic.

The subevents have been chosen in three different ways: (1) Assigning particles with pseudorapidity $0.05 < \eta < 1$ to one subevent and particles with $-1 < \eta < -0.05$ to the other subevent. The "gap" between the two regions ensures that short range correlations, such as Bose-Einstein correlations or Coulomb final state interactions, contribute negligibly to the observed correlation.
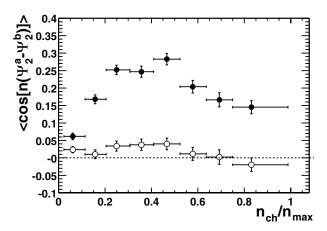
FIG. 2.   Correlation between the event plane angles determined for two independent subevents. The upper set is for the second harmonic ($n = 2$) and the lower set for the first harmonic ($n = 1$). The points are positioned at the values of mean n_{ch}/n_{max} corresponding to each of the centrality bins in Fig. 1. The horizontal bars show the widths of the bins.

(2) Dividing all particles randomly into two subevents. (3) Assigning positive particles to one subevent and negative particles to the other. Figure 2 shows the results for correlation of the event planes of subevents assigned by the pseudorapidity method. The two other methods give similar results. Nonflow effects (not correlated with the reaction plane) would contribute differently for these different subevent choices. The peaked shape of the centrality dependence of $\langle \cos[2(\Psi^a - \Psi^b)] \rangle$ is characteristic of anisotropic flow whereas all known nonflow effects would be monotonic or almost constant for this quantity.

Most commonly discussed nonflow sources of azimuthal correlations are (1) momentum conservation, which can affect directed flow when each subevent is not symmetric about midrapidity and does not affect elliptic flow measurements. (2) Coulomb and Bose-Einstein correlations [23], which are eliminated by the construction of the subevents in Fig. 2. (3) Resonance decay [24], whose effect on the subevent correlation would be independent of centrality. (4) Jets, when calculated using Hijing [22] for the cuts used in the current analysis, give a $\langle \cos[2(\Psi^a - \Psi^b)] \rangle$ of 0.05 for central collisions and lower values for other centralities. This would propagate to a decrease in v_2, but within the systematic errors quoted below. Also, if jets or resonances contribute to second harmonic correlations they would contribute to the first harmonic correlation in a comparable amount [25]. The first harmonic correlation, which is shown in Fig. 2, and the higher harmonics, are significantly weaker than the second harmonic correlation. This sets an upper limit for the contribution of all nonflow effects to the second harmonic correlation and is the basis of the estimate given below of the systematic errors of elliptic flow.

The analysis method involves correlation of the azimuthal angle, ϕ, of each particle with an event plane angle, Ψ, and then averaging over all events. In this paper

we have used three particle correlation methods: (1) Correlating the particles from one hemisphere with the event plane of the subevent in the other hemisphere. (2) Correlating each particle with the event plane of all the *other* particles. (3) Correlating particles of one charge sign with the event plane of the opposite charge sign. The observed elliptic flow comes from the second harmonic Fourier coefficient of the particle azimuthal distribution with respect to the event plane, which is simply $\langle \cos[2(\phi - \Psi_2)] \rangle$. The elliptic flow relative to the real reaction plane, Ψ_R, the plane defined by the impact parameter and the beam, can be evaluated by dividing the observed signal by the resolution, $\langle \cos[2(\Psi - \Psi_R)] \rangle$, of the event plane. The resolutions calculated from the correlation of subevent planes were somewhat different for the different subevent selections, but the resultant v_2 values were the same within statistical errors. The resolutions for the full events reach 0.7 for the centrality at the peak in Fig. 2, while in NA49 [12,13] at the SPS they only reached 0.4. A resolution of the event plane angle of 0.7 is sufficiently close to the ideal value of 1.0, to correlate other quantities, such as two particle correlation measurements (Hanbury-Brown and Twiss) with the event plane. Since we do not measure the correlation with the first harmonic plane, we cannot determine the sign of v_2.

Our analysis procedures have been tested with simulated data [26] to which a known amount of flow has been added. The simulated data were filtered by a GEANT model of STAR and reconstructed in a way similar to that used for the data. For 2% and 10% elliptic flow added to the simulations, the flow extracted was $(2.0 \pm 0.1)\%$ and $(9.7 \pm 0.2)\%$, respectively.

Figure 3 shows v_2 as a function of centrality of the collision. This figure was made with the subevents chosen as in Fig. 2, but the same results within errors were obtained with the other correlation methods. Restricting the primary
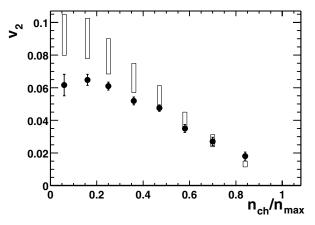

FIG. 3.   Elliptic flow (solid points) as a function of centrality defined as n_{ch}/n_{max}. The open rectangles show a range of values expected for v_2 in the hydrodynamic limit, scaled from ϵ, the initial space eccentricity of the overlap region. The lower edges correspond to ϵ multiplied by 0.19 and the upper edges to ϵ multiplied by 0.25.

vertex z position to reduce TPC acceptance edge effects also made no difference. From the results of the study of nonflow contributions by different subevent selections and the maximum magnitudes of the first and higher-order harmonics, we estimate a systematic error for v_2 of about 0.007, with somewhat smaller uncertainty for the midcentralities where the resolution of the event plane is high. The systematic errors are not included in the figures.

In the hydrodynamic limit, elliptic flow is approximately proportional to the initial space anisotropy, ϵ, which is calculated in Ref. [27]. The transformation to the multiplicity axis in Fig. 3 was done using a Hijing [22] simulation assuming 10% vertex-finding inefficiency for low multiplicity events. In comparing the flow results to ϵ, no unusual structure is evident which could be attributed to the crossing of a phase transition while varying centrality [4,19]. The ϵ values in Fig. 3 are scaled to show the range of hydrodynamic predictions [6,8] for v_2/ϵ from 0.19 to 0.25. The data values for the lower multiplicities could indicate incomplete thermalization during the early time when elliptic flow is generated [5,6]. For the more central collisions, comparison of the data with hydrodynamic calculations suggests that early-time thermalization may be complete. The v_2 values peak at more peripheral collisions than RQMD predictions [18], but in qualitative agreement with hydrodynamic models [7].

The differential anisotropic flow is a function of η and p_t. For the integrated results presented here, all v values should first be calculated as a function of η and p_t, and then $v_2(\eta, p_t)$ should be averaged over either or both variables using the double differential cross sections as weights. Since we do not yet know the cross sections, we have averaged using the observed yields. Figure 4 shows v_2 as a function of p_t for a minimum bias trigger. The η dependence (not shown), which is averaged over p_t from 0.1 to 2.0 GeV/c, is constant at a value of $(4.5 \pm 0.5)\%$ for $|\eta| \lesssim 1.3$. We have assumed that the efficiency (yield/cross section) is constant in the p_t range where the yield is large. This is borne out by studies of the
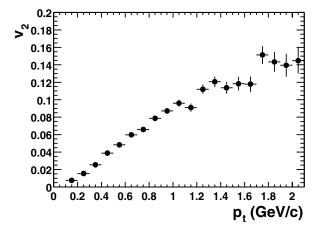
effects of different track quality cuts on the observed p_t spectra. For the p_t dependence the data are not very sensitive to the assumption of constant efficiency as a function of η because v_2 appears to be independent of η in the range used, $|\eta| < 1.3$. Mathematically the v_2 value at $p_t = 0$, as well as its first derivative, must be zero, but it is interesting that v_2 appears to rise almost linearly with p_t starting from relatively low values of p_t. This is consistent with a stronger in-plane hydrodynamic expansion of the system than the average radial expansion. Note that the results shown in Fig. 3 were obtained by taking the average over both η and p_t, weighted by the yield. Although Fig. 4 is for approximately minimum bias data [28] the general shapes are the same for data selected on centrality, except that the slopes of the p_t curves depend on centrality. Figure 4 was made using pseudorapidity subevents, although the same results within errors were obtained using the other two methods.

We conclude that elliptic flow at RHIC rises up to about 6% for peripheral collisions, a value which is more than 50% larger than at the SPS [13], indicating stronger early-time thermalization at this RHIC energy. Elliptic flow appears to be independent of pseudorapidity in the region $|\eta| \lesssim 1.3$. Its p_t dependence is almost linear in the region $0.1 < p_t < 2$ GeV/c. Comparing with estimates [18] based on transport cascade models, we find that elliptic flow is underpredicted by RQMD by a factor of more than 2. Hydrodynamic calculations [6,8] for RHIC energies overpredict elliptic flow by about 20%–50% for the more peripheral collisions. This is just the reverse of the situation at the SPS where RQMD gave a reasonable description of the data and hydrodynamic calculations were more than a factor of 2 too high [13]. Also in contrast to lower collision energies, the observed shape of the centrality dependence of the elliptic flow is similar to hydrodynamic calculations and thus consistent with significant thermalization. The values for elliptic flow compared to hydrodynamic models indicate that early-time thermalization is somewhat incomplete for peripheral collisions but perhaps complete for the more central collisions.

FIG. 4. Elliptic flow as a function of transverse momentum for minimum bias events.

*Deceased.
[1] For reviews and recent developments, see *Quark Matter '99* [Nucl. Phys. **A661** (1999)].

[2] S. Voloshin and Y. Zhang, Z. Phys. C **70**, 665 (1996).

[3] A. M. Poskanzer and S. A. Voloshin, Phys. Rev. C **58**, 1671 (1998).

[4] H. Sorge, Phys. Rev. Lett. **82**, 2048 (1999).

[5] S. A. Voloshin and A. M. Poskanzer, Phys. Lett. B **474**, 27 (2000).

[6] P. Kolb, J. Sollfrank, and U. Heinz, Phys. Rev. C **62**, 054909 (2000).

[7] J.-Y. Ollitrault, Phys. Rev. D **46**, 229 (1992).

[8] P. Kolb, J. Sollfrank, and U. Heinz, Phys. Lett. B **459**, 667 (1999).

[9] D. Teaney and E. V. Shuryak, Phys. Rev. Lett. **83**, 4951 (1999).

[10] E877 Collaboration, J. Barrette *et al.,* Phys. Rev. C **55**, 1420 (1997).

[11] E895 Collaboration, C. Pinkenburg *et al.,* Phys. Rev. Lett. **83**, 1295 (1999).

[12] NA49 Collaboration, H. Appelshäuser *et al.,* Phys. Rev. Lett. **80**, 4136 (1998).

[13] NA49 Collaboration, A. M. Poskanzer and S. A. Voloshin, Nucl. Phys. **A661**, 341c (1999).

[14] WA98 Collaboration, M. M. Aggarwal *et al.,* Phys. Lett. B **403**, 390 (1997); M. M. Aggarwal *et al.,* Nucl. Phys. **A638**, 459 (1998).

[15] J.-Y. Ollitrault, Nucl. Phys. **A638**, 195c (1998).

[16] M. Bleicher and H. Stocker, e-print hep-ph/0006147.

[17] H. Sorge, Phys. Rev. C **52**, 3291 (1995).

[18] R. J. M. Snellings, A. M. Poskanzer, and S. A. Voloshin, STAR Note SN0388, 1999, e-print nucl-ex/9904003.

[19] H. Heiselberg and A.-M. Levy, Phys. Rev. C **59**, 2716 (1999).

[20] STAR Collaboration, K. H. Ackermann *et al.,* Nucl. Phys. **A661**, 681c (1999).

[21] C. Adler *et al.,* e-print nucl-ex/0008005.

[22] M. Gyulassy and X. N. Wang, Comput. Phys. Commun. **83**, 307 (1994); X.-N. Wang and M. Gyulassy, Phys. Rev. D **44**, 3501 (1991).

[23] P. M. Dinh, N. Borghini, and J.-Y. Ollitrault, Phys. Lett. B **477**, 51 (2000).

[24] N. Borghini, P. M. Dinh, and J.-Y. Ollitrault, Phys. Rev. C **62**, 34902 (2000).

[25] Jet quenching could depend on the orientation of the jet with respect to the reaction plane. This would be a real flow correlation. Hijing predicts [18] the effect to be small at midrapidity and $p_t < 2$ GeV/c.

[26] R. L. Ray and R. S. Longacre, STAR Note SN0419, 1999, e-print nucl-ex/0008009.

[27] P. Jacobs and G. Cooper, STAR Note SN0402, 1999, e-print nucl-ex/0008015. The $\varepsilon = \langle y^2 - x^2 \rangle / \langle y^2 + x^2 \rangle$ values used were for a wounded nucleon model with a Woods-Saxon potential.

[28] Approximately, because the quality cuts discriminate somewhat against the more central collisions. At each of the centralities, v_2 was calculated and the values were combined by weighting with the inverse of the square of the errors, which is proportional to the number of particles in that bin. This should be the same as a theoretical calculation of $\langle \cos(2\phi) \rangle$ for all particles in all events.